

Simulation of Natural Convection Influenced by Magnetic Field with Explicit Local Radial Basis Function Collocation Method

K. Mramor¹, R. Vertnik^{2,3}, B. Šarler^{1,3,4,5}

Abstract: The purpose of the present paper is to extend and explore the application of a novel meshless Local Radial Basis Function Collocation Method (LRBFCM) in solution of a steady, laminar, natural convection flow, influenced by magnetic field. The problem is defined by coupled mass, momentum, energy and induction equations that are solved in two dimensions by using local collocation with multiquadrics radial basis functions on an overlapping five noded subdomains and explicit time-stepping. The fractional step method is used to couple the pressure and velocity fields. The considered problem is calculated in a square cavity with two insulated horizontal and two differentially heated vertical walls with magnetic field applied in the horizontal direction. Numerical predictions are calculated for different Grashof numbers, ranging from 10^4 to 10^6 , and Hartman numbers, ranging from 0 to 100, at Prandtl numbers 0.71 and 0.14. The results of the method are compared to predictions, obtained by other numerical methods, including FLUENT [Fluent (2003)]. Good agreement has been achieved. The LRBFCM has been used in this kind of problems for the first time. The main advantage of the method is its simple numerical implementation and no need for polygonisation.

Keywords: Natural convection, magnetohydrodynamics, local radial basis function collocation method, multiquadrics, fractional step method.

1 Introduction

Natural convection [Bejan (1995); Kaviany (2001)] has been extensively studied both experimentally as well as numerically, due to its common occurrence in na-

¹ COBIK, Solkan, Slovenia.

² Štore Steel, Štore, Slovenia.

³ UNG, Nova Gorica, Slovenia.

⁴ IMT, Ljubljana, Slovenia.

⁵ Corresponding author: Professor Božidar Šarler, E-mail: bozidar.sarler@ung.si

ture and technology. It is known that convection in electrically conductive fluid can be significantly suppressed by the application of an external magnetic field [Davidson and Thess (2002); Cheng-Wen, Jian-Fei, Cong-Shan, Sheng-Wei and Da-Chuan (2009); Sarris, Kakarantzas, Grecos and Vlachos (2005)]. [Rudraiah, Barron, Venkatachalappa and Subbaraya (1995)] carried out analysis for differentially heated rectangular cavities with transverse magnetic field for fluids with small Prandtl (Pr) numbers. Similar calculations were performed [Al-Najem, Khanafer and El-Refaee (1998)] for different orientations of the cavity. Several different numerical methods have already been used to solve the problem. Among them are Finite Element Method [Salah, Soulaïmani and Habashi (2001); Sathiyamoorthy and Chamkha (2010); Skala and Barta (2012)], Finite Volume Method (FVM) [Di Piazza and Ciofalo (2002a); Di Piazza and Ciofalo (2002b); Sarris, Kakarantzas, Grecos and Vlachos (2005)], Meshless Local Petrov-Galerkin Method [Arefmanesh, Naja and Nikfar (2010)], Global Radial Basis Function Collocation Method (GRBFCM) [Colaço, Dulikravich and Orlande (2009)], and Meshless Diffuse Approximate Method [Sadat and Couturier (2000)].

A Local Radial Basis Function Collocation Method (LRBFCM) is applied in the present paper to numerically solve the governing equations of the magnetohydrodynamic (MHD) convection problem in a cavity. The idea behind this method is to approximate the function locally over a set of neighboring nodes using Radial Basis Functions (RBFs) [Buhmann (2000)] and to use collocation for determining the expansion coefficients. The method belongs to the class of meshless numerical methods [Atluri and Shen (2002); Atluri (2004); Šarler and Atluri (2010); Gu and Liu (2005); Fasshauer (2007); Liu (2010)] which represent an appealing alternative to the classical numerical methods. Meshless method is a numerical technique that uses a set of scattered nodes [Wendland (2005)], both on the boundary and within the computation domain, to represent the solution of physical phenomena. The main feature of meshless methods is omission of the polygonalisation between the nodes which can be remarkably demanding, particularly in realistic 3D geometrical situations.

The LRBFCM was first proposed in 2006 [Šarler and Vertnik (2006)] for diffusion problems. Since then, it has been successfully applied to various academic and industrial cases, such as diffusion-convection problems with phase change [Vertnik and Šarler (2006)], direct chill casting problems for aluminium alloys with material [Vertnik, Založnik and Šarler (2006)], interface moving boundaries on macroscopic [Kosec and Šarler (2009)] and microscopic [Kovačević and Šarler (2005)] levels, natural convection problems [Kosec and Šarler (2008a); Kosec and Šarler (2008b)], turbulent combined forced and natural convection problems [Vertnik and Šarler (2009), Vertnik and Šarler (2011)], macrosegregation [Kosec, Založnik,

Šarler and Combeau (2011)], natural convection problems with small Pr number [Kosec and Šarler (2012)], continuous casting of steel [Vertnik, Šarler and Senčič (2012)], etc. The method has been applied among others also in solid mechanics problems, such as in bending of composite plates [Ferreira, Roque and Martins (2003)] and large deformation problems such as hot shape rolling of steel [Hanoglu and Šarler (2011)]. The r- and h-adaptive mesh refinements have been developed in [Kovačević and Šarler (2005)] and [Kosec and Šarler (2011)]. Efficient numerical implementation of the method on multiple graphics processing units can be found in [Kosec and Zinterhof (2013)].

Recently, there is a strong development in the direction of combining meshless concepts, based on radial basis functions and finite volume concepts [An-Vo, Mai-Duy and Tran-Cong (2011a, b); An-Vo, Mai-Duy, Tran and Tran-Cong (2013)] as well as RBFs and finite difference concepts [Wright and Fornberg (2006); Bayona, Moscoso, Carretero and Kindelan (2010)]. There is very recently also a strong development in solving multidimensional problems, based on RBFs in one dimension, and iterative alternating direction schemes [Thai-Quang, Mai-Duy, Tran, Tran-Cong (2012); Thai-Quang, Le-Cao, Mai-Duy, Tran-Cong (2012); Ngo-Cong, Mai-Duy, Karunasena, Tran-Cong (2012); Ngo-Cong, Mai-Duy, Karunasena, Tran-Cong (2012)].

LRBFCM is in the present paper extended to MHD flow problems and tested on several examples.

2 Governing Equations

Laminar natural convection flow in domain Ω with boundary Γ of an incompressible Newtonian fluid in the presence of a magnetic field is considered. The governing equations of momentum, mass and energy conservation have the following form:

$$\rho \left[\frac{\partial \mathbf{v}}{\partial t} + \nabla \cdot (\mathbf{v}\mathbf{v}) \right] = -\nabla p + \mu \nabla^2 \mathbf{v} + \mathbf{F}, \quad (1)$$

$$\nabla \cdot \mathbf{v} = 0, \quad (2)$$

$$\frac{\partial T}{\partial t} + \nabla \cdot (\mathbf{v}T) = \alpha \nabla^2 T \quad (3)$$

where \mathbf{v} is the velocity, p pressure, μ viscosity, α thermal diffusivity and T stands for temperature of the fluid. In order to describe the influence of magnetic field and buoyancy on the fluid flow, a body force term $\mathbf{F} = \mathbf{F}_b + \mathbf{F}_m$ is used. \mathbf{F}_b describes thermal Boussinesq buoyancy force $\mathbf{g}\rho\beta_T(T - T_{ref})$, where \mathbf{g} is gravitational acceleration, ρ is the considered constant reference density of the fluid, β_T is thermal

expansion coefficient, and T_{ref} is reference temperature. $\mathbf{F}_m = \mathbf{j} \times \mathbf{B}$ describes the Lorentz force, expressed from the total current density (given by Ohm's law)

$$\mathbf{j} = \mathbf{j}_d + \mathbf{j}_i; \quad \mathbf{j}_d = -\sigma \nabla \varphi, \quad \mathbf{j}_i = \sigma (\mathbf{v} \times \mathbf{B}), \quad (4)$$

where σ , φ , and \mathbf{B} represent fluid's electric conductivity, electric potential, and applied magnetic field, respectively. \mathbf{j}_i is induced electric current density, which is a consequence of electric charge displacement that happens as a result of charges moving due to the applied magnetic force. \mathbf{j}_d is diffusive electric current, pointing in an opposite direction to \mathbf{j}_i , which is a consequence of charge separation. The direction of \mathbf{j} can point in the direction of either of its components \mathbf{j}_i and \mathbf{j}_d . Lorentz force can either aid or oppose the flow motion depending on which term (inductive or diffusive) in current density prevails. By considering that the electric charge must be preserved ($\nabla \cdot \mathbf{j} = 0$), electric potential can be calculated from Poisson's equation

$$\nabla^2 \varphi = \nabla \cdot (\mathbf{v} \times \mathbf{B}). \quad (5)$$

The governing equations (1, 2, 3) are solved in two dimensions. For this purpose, Cartesian coordinate system with base vectors \mathbf{i}_x , \mathbf{i}_y and coordinates x , y is introduced. Since the Lorentz force is calculated from the cross product, the velocity vector \mathbf{v} and magnetic field density \mathbf{B} are written in three-dimensions with the assumption that the third coordinate equals 0 ($\mathbf{v} = v_x \mathbf{i}_x + v_y \mathbf{i}_y$, $\mathbf{B} = B_x \mathbf{i}_x$), thus resulting in a Lorentz force that is written as follows $\mathbf{F}_m = \sigma v_y B_x^2 \mathbf{i}_y$. Such a situation is thus reduced to two dimensions.

The magnetic Reynolds number Re_m is defined as

$$Re_m = v_0 \ell \mu_0 \sigma, \quad (6)$$

where v_0 is characteristic velocity, μ_0 is magnetic permeability of free space and ℓ is characteristic length. It indicates whether the magnetic advection or magnetic diffusion term has more influence. It is assumed here that $Re_m \ll 1$, which means that the induction is negligible in comparison to the applied magnetic field. Small magnetic Reynolds number $Re_m \ll 1$ is in practice applicable in liquid-metal magnetohydrodynamics (MHD), which is the target application direction of the present research. In this situation, the induced magnetic field remains very small in comparison to the applied magnetic field. The magnetic field thus relaxes towards a purely diffusive state, determined by boundary conditions. The inhomogeneities in the field are smoothed out.

2.1 Boundary and initial conditions

In the present paper, the domain Ω is considered to be a square cavity. The configuration of the problem is presented in Fig. 1. We seek the solution (p, T, \mathbf{v}) of mass (Eq. 2), momentum (Eq. 1) and energy conservation (Eq. 3) equations at time $t_0 + \Delta t$ by assuming the known initial velocity \mathbf{v}_0 , temperature T_0 and pressure p_0 fields at time t_0 , and the boundary conditions that follow.

The velocity boundary conditions on all the walls are non-permeable and non-slip

$$v_x = 0, \quad v_y = 0. \quad (7)$$

The top and the bottom walls are adiabatic, the temperature boundary conditions on these two walls are

$$\frac{\partial T}{\partial \mathbf{n}} = 0. \quad (8)$$

The temperatures on the left and right walls have predetermined uniform values; the temperature on the left wall is T_H , considered higher than the temperature on the right wall T_C . Both temperatures are kept constant throughout the process. The boundary condition for electric potential (Eq. 5) at the sides of the square Γ are given by

$$\frac{\partial \phi}{\partial \mathbf{n}} = (\mathbf{v} \times \mathbf{B}) \cdot \mathbf{n} \quad (9)$$

for an insulating boundary, where \mathbf{n} is normal to the boundary. It is assumed here that all the walls have insulating boundaries. The electric potential boundary condition is therefore

$$\frac{\partial \phi}{\partial \mathbf{n}} = 0 \quad (10)$$

as the velocities on the boundary are 0. The initial values for pressure, temperature, velocity and predetermined magnetic field are given as $p = 0$, $T_{ref} = \frac{T_H - T_C}{2}$, $v_x = 0$, $v_y = 0$, $B_x = 1$, and $B_y = 0$.

The magnetohydrodynamic flow in a square cavity of the size L is characterized by the following dimensionless parameters (with $\ell=L$)

$$Ra = \frac{g\beta_T(T_H - T_C)\ell^3}{\nu\alpha}, \quad (11)$$

$$Pr = \frac{\nu}{\alpha}, \quad (12)$$

$$Ha = B\ell\sqrt{\frac{\sigma}{\mu}}, \tag{13}$$

$$Gr = \frac{Ra}{Pr}, \tag{14}$$

and Re_m (Eq. 6). Nusselt number (Nu), defined as

$$Nu = \int_0^L \frac{\partial T}{\partial x} \Big|_{x=0} dy, \tag{15}$$

is used to compare the results, obtained with the developed LRBFCM to the results obtained with the published reference results [Colaço, Dulikravich and Orlande (2009); de Vahl Davis (1983)] or those obtained with FLUENT. The stream function Ψ is calculated by integrating the velocity

$$\Psi(x, y) = \int_0^y v_x(x, \tilde{y}) d\tilde{y}. \tag{16}$$

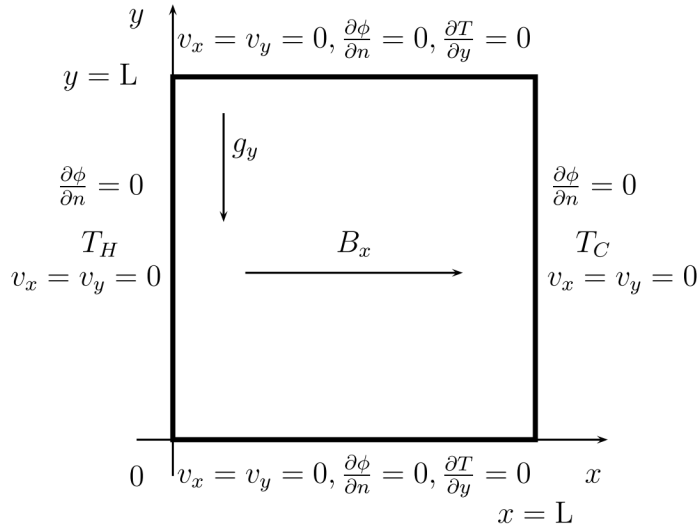


Figure 1: Scheme of the computational domain and boundary conditions of a two-dimensional differentially heated cavity. Top and bottom walls are insulated. The magnetic field is applied in horizontal direction.

3 Solution procedure

The solution procedure is based on two-level explicit timestepping. It is first explained in a setting, where no reference needs to be made regarding the space discretisation, that is explained afterwards. The Fractional Step Method (FSM) of [Chorin (1967)] is used for pressure velocity coupling. The solution procedure begins with calculation of the initial body force term $\mathbf{F}_0 = [-g\mathbf{i}_y\rho\beta_T(T - T_{ref}) + \sigma v_y B_x^2 \mathbf{i}_y]_0$. The intermediate velocity \mathbf{v}^* is afterwards calculated without the pressure gradient

$$\mathbf{v}^* = \mathbf{v}_0 + \frac{\Delta t}{\rho} [-\rho\nabla \cdot (\mathbf{v}\mathbf{v}) + \mu\nabla^2 \mathbf{v} + \mathbf{F}]_0, \quad (17)$$

where index 0 stands for initial conditions at time $t = t_0$. Poisson equation is than used to calculate the pressure

$$\nabla^2 p = \frac{\rho}{\Delta t} \nabla \cdot \mathbf{v}^* = S. \quad (18)$$

The following Neumann boundary conditions are used to solve the pressure Poisson equation above

$$\frac{\partial p}{\partial \mathbf{n}} = \mathbf{0}. \quad (19)$$

The final velocity components are corrected by the pressure gradient

$$\mathbf{v} = \mathbf{v}^* - \frac{\Delta t}{\rho} \nabla p. \quad (20)$$

The energy equation is calculated as

$$T = T_0 + \frac{\Delta t}{\rho} [-\rho\nabla \cdot (\mathbf{v}T) + \nabla \cdot (\alpha\nabla T)]_0. \quad (21)$$

The LRBFCM [Šarler and Vertnik (2006)] method is used in the present paper to handle the partial derivatives. LRBFCM is a numerical technique for solving partial differential equations through a local interpolation of function and its derivatives over a set of neighbouring nodes by radial basis functions. The region is discretised into N calculation points, of which there are N_Ω domain and N_Γ boundary points. The region is divided into N overlapping subdomains, each of which consists of ${}_l M$ (in general) non-equally spaced nodes ${}_l \mathbf{p}_n$, where $l = 1, \dots, N$ stands for subdomain and $n = 1, \dots, {}_l M$.

Approximation of function θ is represented on a local subdomain, as a linear combination of Radial Basis Functions (RBF)

$$\theta({}_l\mathbf{p}_n) = \sum_{i=1}^M {}_l\psi_i({}_l\mathbf{p}_n){}_l\gamma_i, \tag{22}$$

where M stands for a number of shape functions, ${}_l\gamma_i$ for an expansion coefficient, ${}_l\psi_i$ for shape functions, centred in points ${}_l\mathbf{p}_n$. The influence domain of the node ${}_l\mathbf{p}_n$ consists of the ${}_lM - 1$ nodes nearest to the node ${}_l\mathbf{p}_n$. A five-noded overlapping subdomain is used in this paper (Fig. 2). By considering the collocation condition

$${}_l\theta({}_l\mathbf{p}_n) = {}_l\theta_i \tag{23}$$

and Eq. 22, a linear system of M equations is obtained

$${}_l\boldsymbol{\psi}_l\boldsymbol{\gamma} = {}_l\boldsymbol{\theta}. \tag{24}$$

The expansion coefficients ${}_l\boldsymbol{\gamma}$ can only be determined by collocation when the number of domain nodes ${}_lM$ matches the number of the basis functions M and when the basis functions matrix is non-singular [Hon and Schaback (2001)]. The expansion coefficients can than be determined by inverting the matrix ${}_l\boldsymbol{\psi}$

$${}_l\boldsymbol{\gamma} = {}_l\boldsymbol{\psi}_l^{-1}{}_l\boldsymbol{\theta}. \tag{25}$$

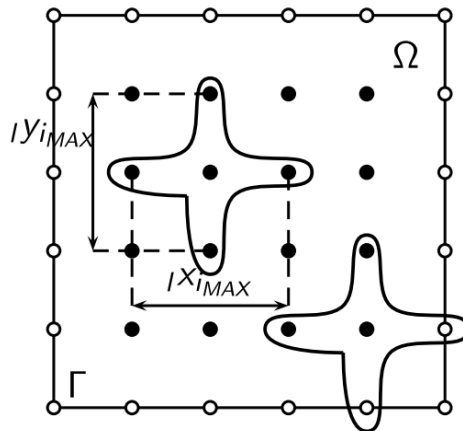


Figure 2: Scheme of the discretisation. The Γ , Ω , ${}_lX_{iMAX}$ and ${}_lY_{iMAX}$ represent boundary, domain and scaling parameters in x and y direction respectively. Empty dots represent boundary points whereas black dots represent domain points.

By considering Eq. 25, ${}_l\theta(\mathbf{p})$ can be expressed as

$$\theta(\mathbf{p}) = \sum_{i=1}^M {}_l\psi_i(\mathbf{p}) \sum_{k=1}^M {}_l\psi_{ik}^{-1}(\mathbf{p}) {}_l\theta_k \tag{26}$$

One of the most commonly used RBFs are multiquadrics (MQ) [Franke (1982)]

$${}_l\psi_i(\mathbf{p}) = \sqrt{{}_lr_i^2(\mathbf{p}) + c^2} \tag{27}$$

where c stands for dimensionles shape parameter, which is, in our case, predetermined and set to 32 in all the cases. r_i is scaled as

$${}_lr_i(\mathbf{p}) = \sqrt{\left(\frac{x - x_i}{{}_lx_{i\max}}\right)^2 + \left(\frac{y - y_i}{{}_ly_{i\max}}\right)^2} \tag{28}$$

where ${}_lx_{i\max}$, and ${}_ly_{i\max}$ are in general different scaling parameters in each of the subdomains in x and y directions respectively (Fig. 2).

As a means to solve the partial differential equations of the model, the first and the second derivatives of function $\theta(\mathbf{p})$ have to be calculated on the influence domain. The operator applied on the approximated function is expressed by [Kansa (1990a,b)]

$$\frac{\partial^j}{{}_l\chi^j} {}_l\theta(\mathbf{p}) = \sum_{i=1}^M {}_l\gamma_i \frac{\partial^j}{{}_l\chi^j} {}_l\psi_i(\mathbf{p}) \tag{29}$$

where the index j is used to denote the order of derivative (1 or 2) and $\chi = x, y$. Eq. 17 and Eq. 21 are solved as indicated above.

For the solution of Poisson equation (Eq. 18) a sparse matrix is used. The subdomain points ${}_l\mathbf{p}_n$ coincide with the global points \mathbf{p}_i . The relation between the indexes is considered as follows $\mathbf{p}_{i(l,n)} = {}_l\mathbf{p}_n$. The pressure is represented on each of the subdomains by RBFs and their coefficients

$$p(\mathbf{p}) = \sum_{n=1}^M \psi_{i(l,n)}(\mathbf{p}) {}_l\gamma_n. \tag{30}$$

The expansion coefficients ${}_l\gamma$ are determined by collocation as shown in Eq. 25 and the pressure is thus

$$p_{i(l,m)} = \sum_{n=1}^M {}_l\Psi_{mn} {}_l\gamma_n; m = 1, \dots, M. \tag{31}$$

The pressure can than be calculated in each of the subdomains as

$$p(\mathbf{p}) = \sum_{n=1}^M \sum_{m=1}^M {}_l \Psi_{i(l,n)}(\mathbf{p}) {}_l \Psi_{nm}^{-1} p_{i(l,m)}. \quad (32)$$

The collocation in global point \mathbf{p}_k results in

$$\sum_{j=1}^N \Psi_{lj} p_j = S_l, \quad (33)$$

where Ψ_{lj} is the the global sparse matrix element.

Lastly, the velocity components, temperature, pressure and body force are updated for each node and the solution is ready for the next time step. The calculation is stopped when the following steady state conditions are achieved in each of the N calculation points

$$|\mathbf{v}_i - \mathbf{v}_{i0}| < \varepsilon_v, \quad |T_i - T_{i0}| < \varepsilon_T, \quad |p_i - p_{i0}| < \varepsilon_p, \quad i = 1, \dots, N \quad (34)$$

where \mathbf{v}_{i0} and \mathbf{v}_i , T_{i0} and T_i , p_{i0} and p_i and are the two consecutive velocity, temperature and pressure values, respectively. The criteria are set to $\varepsilon_v = 10^{-6}$, $\varepsilon_T = 10^{-6}$, $\varepsilon_p = 10^{-6}$. A detailed description of the solution procedure for turbulent flow by the FSM can be found in [Vertnik and Šarler (2009)].

4 Numerical implementation

The method has been implemented in Fortran and executed on Intel Core i7 CPU, 2.8 GHz computer under 64 bit Windows 7 operating system. The heat and mass transfer are calculated with solver coded in Fortran by the second author. The MHD module is added to the solver by the first author. The sparse matrix, used to calculate the pressure, is solved with Pardiso routine and Intel Math Kernel Library 11. OpenMP is used for parallelization. The postprocessing is done in Octave 3.6.1 and Gnuplot 4.4. The Nusselt number (Eq. 15) is calculated from final temperatures with Simpson's 3/8 rule. The 4-th order Runge-Kutta is used for numerical integration of the stream function (Eq. 16).

5 Numerical examples

Three different tests are performed to verify the numerical method. The first test case (Case 1) describes the standard de Vahl Davis benchmark test [de Vahl Davis (1983)] with the absence of magnetic field. The second test case (Case 2) describes stable, laminar fluid flow in a square cavity under the influence of magnetic field.

The most common reference papers for the defined problem, use $Pr=0.71$ [Colaço, Dulikravich and Orlande (2009)], which is a Prandtl number typical for air. In the third test case (Case 3) the MHD flow with $Pr=0.14$, (typical for steel), is used. Each of the three cases is compared to the results obtained from commercial code FLUENT or the results obtained from a pertained reference paper.

The node arrangement is refined near the walls in all of the cases (Fig. 3). The non-uniformity is obtained in the following way. The uniform node arrangement in x -direction of the square is given by

$$x_i^{uniform} = x_{min} + (i - 1) \frac{x_{max} - x_{min}}{N - 1}, \quad i = 1, 2, \dots, N, \quad (35)$$

where $x_{min} = 0$ and $x_{max} = L$ are the position of the first and the last node. It is first normalized to the interval $[0,1]$

$$x_{i,norm}^{uniform} = \frac{x_i^{uniform} - x_{min}}{x_{max} - x_{min}} \quad (36)$$

and than refined as

$$x_{i,norm}^{refined} = 1.0 - (1.0 - x_{i,norm}^{uniform})^b, \quad (37)$$

with b standing for the refinement parameter. Finally, the refinement is rescaled to the original interval

$$x_i^{refined} = x_{min} + x_{i,norm}^{refined} L. \quad (38)$$

A non-uniform node arrangement is set in a similar way in y direction as well. The refinement $b = 1.2$ is used in all of the cases.

All the results are presented in their dimensionless form

$$x' = \frac{x}{L}, \quad y' = \frac{y}{L}, \quad \mathbf{v}' = \frac{\mathbf{v}L}{\alpha}, \quad p' = \frac{pL^2}{\rho\alpha^2}, \quad \Theta = \frac{T - T_C}{T_H - T_C}, \quad t' = \frac{t\alpha}{L^2}, \quad (39)$$

where x' , y' , \mathbf{v}' , p' , Θ , t' are dimensionless coordinates, velocities, pressure, temperature, and time, respectively.

5.1 Case 1

Case 1 is the well known de Vahl Davis benchmark test [de Vahl Davis (1983)]. As the purpose of this paper is to investigate the MHD flow, which is characterised by small Pr numbers, de Vahl Davis benchmark test is presented here only as a basic test of the accuracy of the method. The influence of magnetic field on the fluid flow

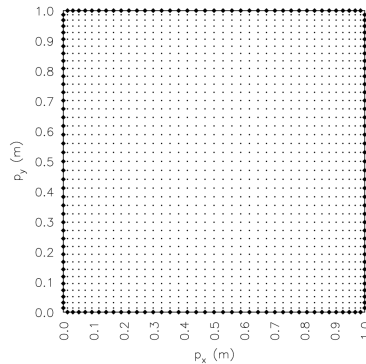


Figure 3: Scheme of the node arrangement for 41x41. Dots represent domain nodes and black diamonds represent boundary nodes.

Table 1: Overview and definition of the involved test cases.

| case | Pr | Ra | Gr | Ha | Δt [s] |
|------|------|--------|--------|-----|----------------|
| 1 a | 0.71 | 10^3 | / | / | 10^{-5} |
| 1 b | 0.71 | 10^4 | / | / | 10^{-5} |
| 1 c | 0.71 | 10^5 | / | / | 10^{-5} |
| 1 d | 0.71 | 10^6 | / | / | 10^{-5} |
| 2 a | 0.71 | / | 10^4 | 0 | 10^{-5} |
| 2 b | 0.71 | / | 10^4 | 10 | 10^{-6} |
| 2 c | 0.71 | / | 10^4 | 50 | 10^{-6} |
| 2 d | 0.71 | / | 10^6 | 0 | 10^{-5} |
| 2 e | 0.71 | / | 10^6 | 10 | 10^{-6} |
| 2 f | 0.71 | / | 10^6 | 50 | 10^{-6} |
| 2 g | 0.71 | / | 10^6 | 100 | 10^{-6} |
| 3 a | 0.14 | / | 10^4 | 0 | 10^{-5} |
| 3 b | 0.14 | / | 10^4 | 10 | 10^{-6} |
| 3 c | 0.14 | / | 10^4 | 50 | 10^{-6} |
| 3 d | 0.14 | / | 10^5 | 0 | 10^{-5} |
| 3 e | 0.14 | / | 10^5 | 10 | 10^{-6} |
| 3 f | 0.14 | / | 10^5 | 50 | 10^{-6} |
| 3 g | 0.14 | / | 10^5 | 100 | 10^{-6} |
| 3 h | 0.14 | / | 10^6 | 0 | 10^{-5} |
| 3 i | 0.14 | / | 10^6 | 10 | 10^{-6} |
| 3 j | 0.14 | / | 10^6 | 50 | 10^{-6} |
| 3 k | 0.14 | / | 10^6 | 100 | 10^{-6} |
| 3 l | 0.14 | / | 10^6 | 200 | 10^{-6} |

is investigated in the successive sections. The results are calculated on 101x101 node arrangement and compared to the results from [de Vahl Davis (1983)] and [Kosec and Šarler (2008b)] presented in Tab. 2. The results calculated with present LRBFCM are in terms of Nu slightly larger than those obtained by [Kosec and Šarler (2008b)] who used LRBFCM with local pressure correction and slightly smaller than those from [de Vahl Davis (1983)]. The difference between the present results and the results from [Kosec and Šarler (2008b)] is probably due to different node arrangement; in the present case a non-uniform node arrangement is used, whereas in [Kosec and Šarler (2008b)] a uniform node arrangement is employed. The results are also compared with the results obtained with the global RBFCM [Šarler (2005)]. A slight difference between the present results and the results calculated in [Šarler (2005)] is mainly due to very much different node densities. In the present case a 101x101 node arrangement is used whereas in [Šarler (2005)] a much coarser 30x30 node arrangement is employed. It should be noted that the global RBFCM would fail for node arrangement 101x101 due to the ill conditioning of the global collocation matrix.

Table 2: Case 1. A comparison of LRBFCM predictions with previous solutions for $Pr=0.71$ and various Ra numbers.

| Ra | Nu present | Nu [de Vahl Davis (1983)] | Nu[Kosec and Šarler (2008b)] | Nu [Šarler (2005)] |
|--------|------------|---------------------------|------------------------------|--------------------|
| 10^3 | 1.108 | 1.116 | 1.089 | 1.114 |
| 10^4 | 2.223 | 2.234 | 2.258 | 2.246 |
| 10^5 | 4.497 | 4.510 | 4.511 | 4.523 |
| 10^6 | 8.779 | 8.798 | 8.970 | 8.834 |

5.2 Case 2

Case 2 tackles a steady, laminar fluid flow in a square cavity. The flow is described with a relatively high Prandtl number $Pr=0.71$, which is otherwise typical for air. It is assumed here that the fluid is conductive despite atypically high Pr number. The results of this test case are compared with the results obtained in [Colaço, Dukravich and Orlande (2009)] and those calculated with FLUENT. The Ha number is varied from 0 to 100 ($Ha = 0, 10, 50, 100$) and the Gr number varies from 10^4 to 10^6 ($10^4, 10^5, 10^6$).

The results are summarized in Tab. 3, where the RBFCM data from [Colaço, Dukravich and Orlande (2009)] are compared to the results calculated with LRBFCM. As can be seen in the Tab. 3, Nu decreases with increasing Ha. The values of

the results obtained with LRBFCM in terms of Nu are slightly higher than the results obtained with RBF method used in [Colaço, Dulikravich, and Orlande (2009)] and slightly smaller than the results obtained with FVM method (FLUENT). The Nu number is further compared for three different node arrangements with 41x41, 61x61, 81x81 and 101x101 nodes as shown in Fig. 4. Nu is slightly larger for the smallest node arrangement (41x41), but is almost the same for node arrangements with 61, 81 and 101 nodes in each direction. As the Nu does not change significantly for node arrangements with larger number of the nodes, the calculations are considered reasonably independent on the node arrangement in case when 81x81 nodes are used. All of the subsequent calculations are therefore performed for 81x81 node arrangement, whereas in [Colaço, Dulikravich, and Orlande (2009)] the calculations are done on very coarse 15x15 and 25x25 node arrangements. Finally, velocity and temperature profiles along the horizontal line through the center of the cavity are presented in Fig. 5 and 6. As can be seen in Fig. 5 and 6, the results obtained in [Colaço, Dulikravich, and Orlande (2009)] and FLUENT are in good agreement with those calculated with LRBFCM. The node arrangement in FLUENT and in [Colaço, Dulikravich, and Orlande (2009)] are nonuniform and refined near the wall by $b=1.2$, similar as in the present node arrangement. In [Colaço, Dulikravich, and Orlande (2009)], dimensionless velocity is calculated as $\mathbf{v}' = \mathbf{v} [g\beta(T_H - T_C)L]^{-1/2}$. The streamlines and isotherms were first visually compared to [Colaço, Dulikravich, and Orlande (2009)]. The results seem to qualitatively agree. The quantitative comparison of the Nu results is given in Tab. 3.

Table 3: Case 2. Comparison of present predictions with previous works in terms of Nu for Pr=0.71 and various Ha and Gr numbers. [1]: present, [2]: [Colaço, Dulikravich, and Orlande (2009)], [3]: FLUENT.

| Ha | Nu [1] | Nu [2] | Nu [3] |
|--------------------|--------|--------|--------|
| Gr=10 ⁴ | | | |
| 0 | 2.03 | 2.02 | 2.06 |
| 10 | 1.71 | 1.70 | 1.84 |
| 50 | 1.01 | 1.00 | 1.06 |
| Gr=10 ⁶ | | | |
| 0 | 8.15 | 9.21 | 7.98 |
| 10 | 7.99 | 9.04 | 7.88 |
| 100 | 3.33 | 3.54 | 4.27 |

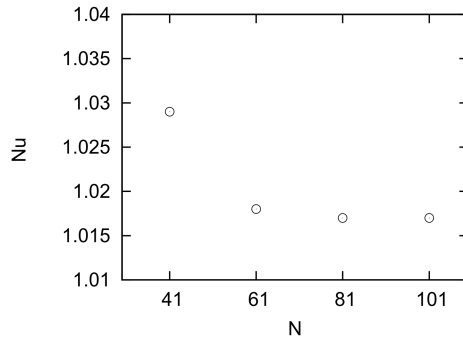


Figure 4: Case 2. Nu as a function of four different node arrangements (41x41, 61x61, 81x81 and 101x101) at $Gr=10^4$ and $Pr=0.71$.

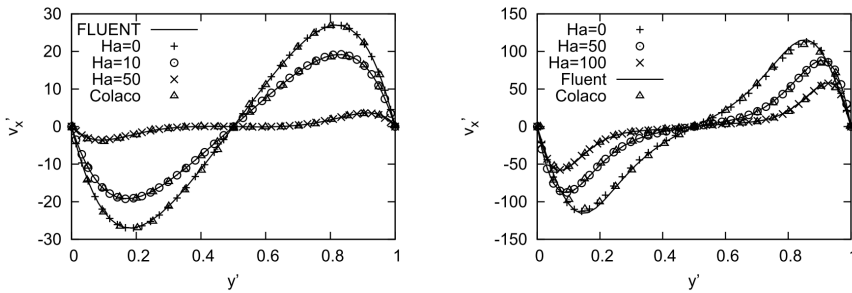


Figure 5: Case 2. Comparison of dimensionless velocities v'_x for $Gr=10^4$ (left) and $Gr=10^6$ (right) along the horizontal line through the center of the cavity.

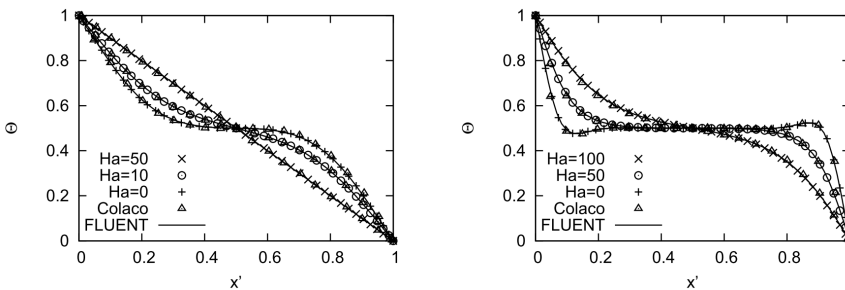


Figure 6: Case 2. Comparison of dimensionless temperatures Θ for $Gr=10^4$ (left) and $Gr=10^6$ (right) along the horizontal line through the center of the cavity.

5.3 Case 3

Case 3 represents a more realistic MHD flow test case. A stable, laminar fluid flow is described in square cavity for steel typical $Pr=0.14$ ($\mu = 0.006\text{kg}/(\text{ms})$, $\rho = 7200\text{kg}/\text{m}^3$, $\alpha = 30\text{W}/(\text{mK})$) and different Ha and Gr numbers. Due to the lack of relevant published data, the results are compared solely with the results calculated with FLUENT.

The results are calculated for Ha values of 0, 10, 50, 100 and 200 and for Gr values of 10^4 , 10^5 and 10^6 . As can be seen in Fig. 7, 8, 9, 10 and 11 are the results calculated with in-house LRBFCM and with FLUENT in a very good agreement. The temperature profile along the horizontal line through the center of the cavity is depicted in Fig. 7 and 8. They show that by increasing the Gr number the profile changes; the temperature gradient at both sides of the cavity increases, and consequently the temperature gradient in the middle of the cavity decreases, which results in a thicker boundary layer. It can also be seen that by increasing the Ha number the convection is quenched; the higher the Ha number is, the more the isotherms are straightened and parallel with the vertical walls of the cavity.

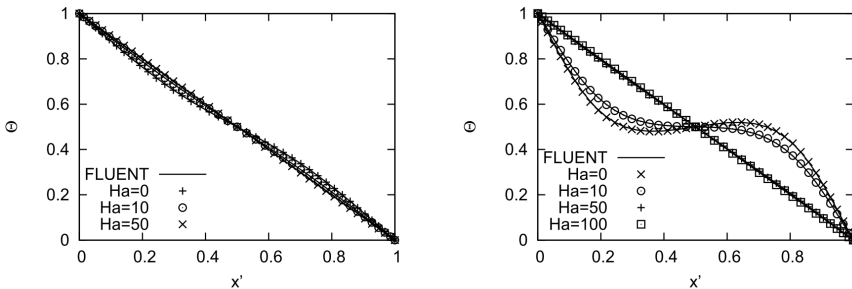


Figure 7: Case 3. Comparison of dimensionless temperatures Θ for $Gr=10^4$ (left) and $Gr=10^5$ (right) along the horizontal line through the center of the cavity.

Fig. 9, 10 and 11 show dimensionless velocities v'_x and v'_y along the horizontal and the vertical line through the center of the cavity. Both velocity components are quenched due to the externally applied magnetic field. The external magnetic field has to be stronger for higher Gr numbers in order to annihilate the fluid flow.

Fig. 12 and 13 depict streamlines for various Gr and Ha numbers. In the presence of weak magnetic field, the streamlines are similar to those in the case without the magnetic field. By increasing the magnetic field, the streamlines become tilted and elongated. For a sufficiently large Ha numbers, the retarding effect of Lorentz's force completely quenches convection. Fig. 14 and 15 depict isotherms for various

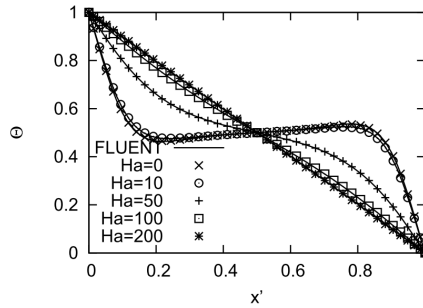


Figure 8: Case 3. Comparison of dimensionless temperatures Θ for $Gr=10^6$ along the horizontal line through the center of the cavity.

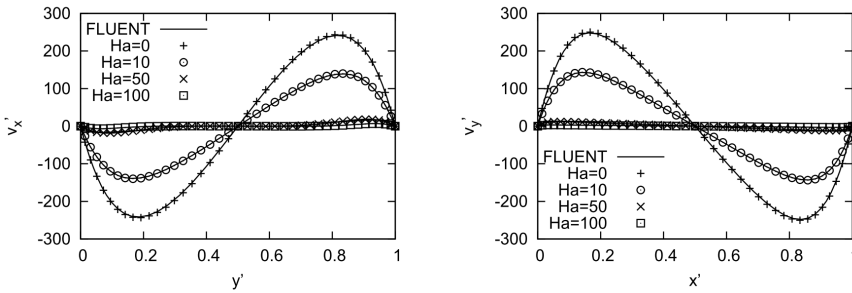


Figure 9: Case 3. Comparison of v'_x along the horizontal (left) and v'_y along the vertical lines (right) through the center of the cavity for $Gr=10^4$ as a function of different Ha .

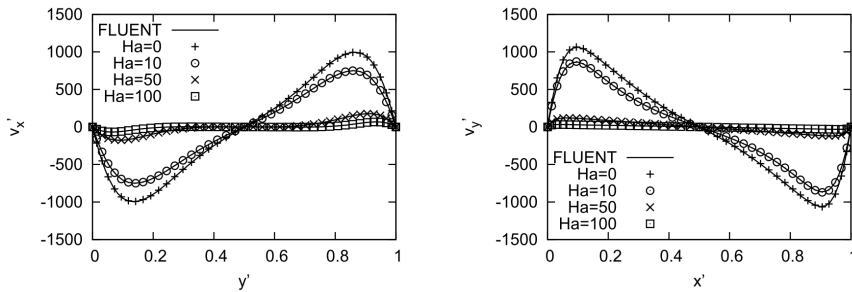


Figure 10: Case 3. Comparison of v'_x along the horizontal (left) and v'_y along the vertical lines (right) through the center of the cavity for $Gr=10^5$ as a function of different Ha .

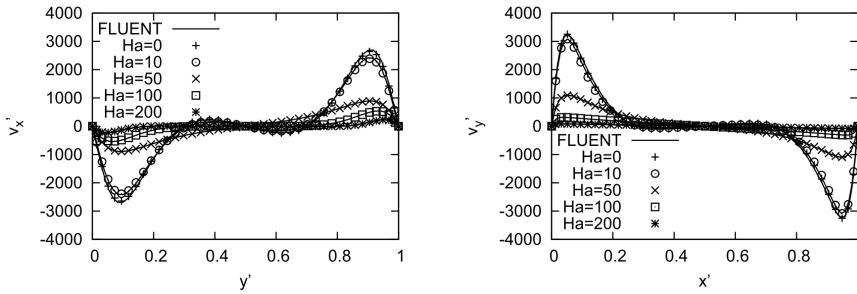


Figure 11: Case 3. Comparison of v'_x along the horizontal (left) and v'_y along the vertical lines (right) through the center of the cavity for $Gr=10^6$ as a function of different Ha .

Gr and Ha numbers. The convection is suppressed and the magnetic field thus decreases the heat transfer rate between the hot and the cold walls. The streamlines and isotherms were visually compared to those calculated with FLUENT. The values of dimensionless velocities are given in Tab. 4 (v'_x and v'_y) for $Gr=10^6$ and $Ha=0$ and $Ha=50$.

Table 4: Case 3. Tabulated dimensionless velocities for $Gr = 10^6$, $Ha=0$ and 50. (See also Fig. 11), obtained by LRBFCM.

| x (in actual nodal points) | v'_x | v'_y | v'_x | v'_y |
|----------------------------|----------------------|----------------------|-----------------------|-----------------------|
| | $Gr=10^6,$ $Ha=0$ | $Gr=10^6,$ $Ha=0$ | $Gr=10^6,$ $Ha=50$ | $Gr=10^6,$ $Ha=50$ |
| 0.0000 | 0.0000 | 0.0000 | 0.0000 | 0.0000 |
| 0.0513 | -2118.4 | 3230.0 | -762.79 | 1092.6 |
| 0.1179 | -2480.2 | 1865.8 | -861.00 | 841.29 |
| 0.1665 | -1695.4 | 957.14 | -717.00 | 615.38 |
| 0.2176 | -821.50 | 332.76 | -548.51 | 430.96 |
| 0.2708 | -194.71 | 20.478 | -397.38 | 291.58 |
| 0.3259 | 144.73 | -102.16 | -271.57 | 188.84 |
| 0.3825 | 244.16 | -93.843 | -168.14 | 112.34 |
| 0.4406 | 168.41 | -50.000 | -80.286 | 52.309 |
| 0.5000 | -0.1860 | 0.0128 | 0.1889 | 0.1202 |

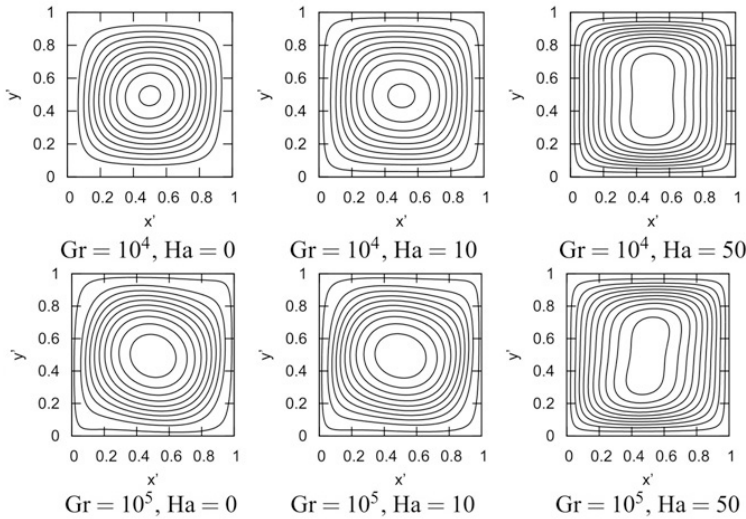


Figure 12: Case 3. Comparison of streamlines at various Gr and Ha numbers. The streamlines are equidistantly spaced. The maximum values of streamlines are: 2.55 ($Gr = 10^4, Ha = 0$), 3.3 ($Gr = 10^4, Ha = 10$), 0.24 ($Gr = 10^4, Ha = 100$), 20.2 ($Gr = 10^5, Ha = 0$), 15.2 ($Gr = 10^5, Ha = 10$), and 2.4 ($Gr = 10^5, Ha = 50$).

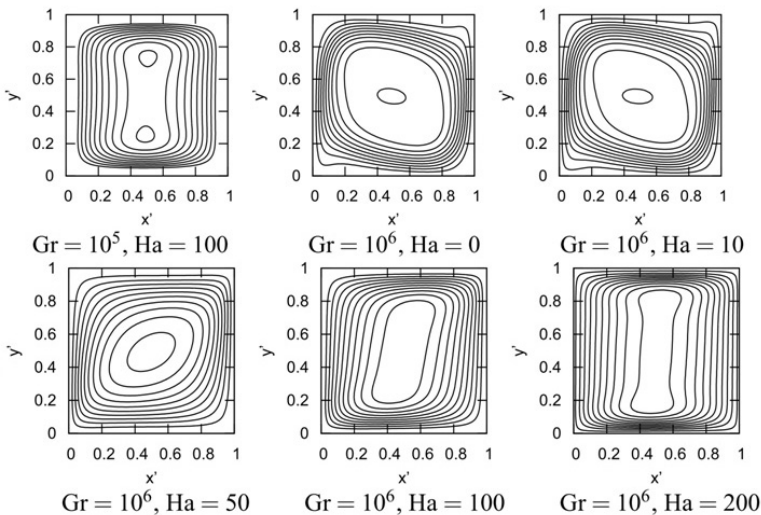


Figure 13: Case 3. Comparison of streamlines at various Gr and Ha numbers. The streamlines are equidistantly spaced. The maximum values of streamlines are: 0.65 ($Gr = 10^5, Ha = 100$), 34.0 ($Gr = 10^6, Ha = 0$), 29.0 ($Gr = 10^6, Ha = 10$), 16.0 ($Gr = 10^6, Ha = 50$), 5.5 ($Gr = 10^6, Ha = 100$), and 1.55 ($Gr = 10^6, Ha = 200$).

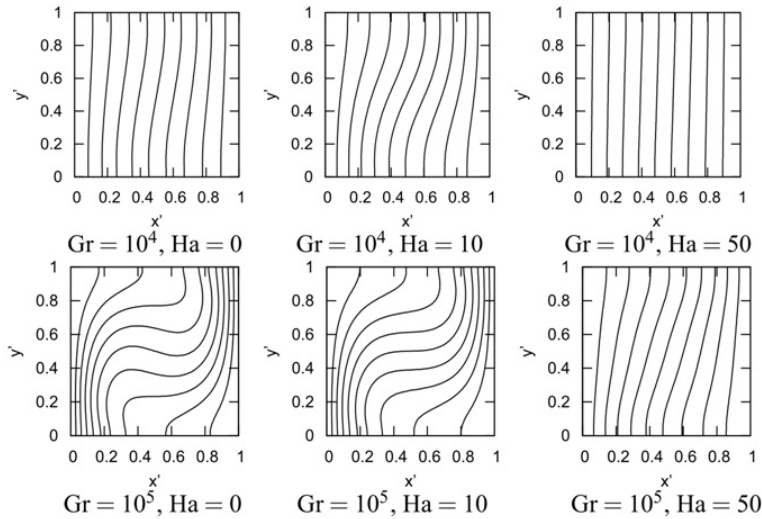


Figure 14: Case 3. Isotherms at various Gr and Ha numbers at $Pr=0.14$. The isotherms are equidistantly spaced, the minimum is at T_C (right boundary) and the maximum T_H (left boundary).

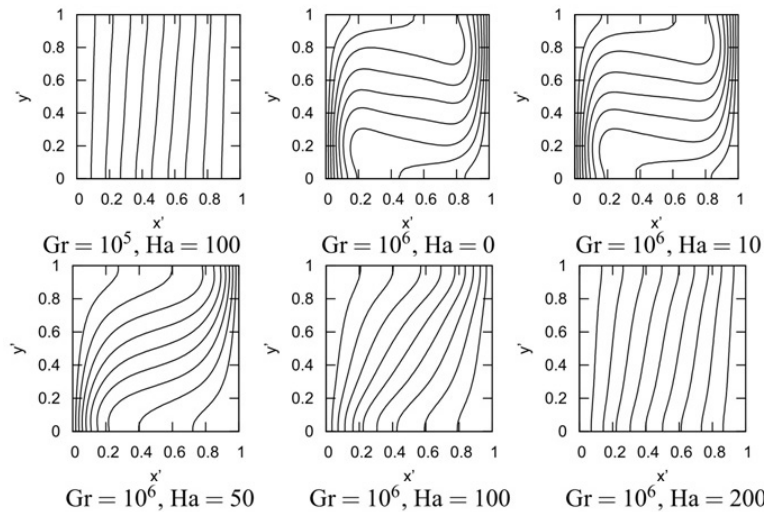


Figure 15: Case 3. Isotherms at various Gr and Ha numbers at $Pr=0.14$. The isotherms are equidistantly spaced, the minimum is at T_C (right boundary) and the maximum at T_H (left boundary).

6 Conclusions

A new meshless method, based on LRBFCM and FSM, for solving MHD convection in a square cavity is proposed. The method is first verified for natural convection in the absence of magnetic field [de Vahl Davis (1983)] and then for natural convection flow under the influence of external magnetic field [Colaço, Dulikravich and Orlande (2009), Garandet, Alboussiere and Moreau (1992)]. Next, the results of the deduced method are tested against the results obtained with FLUENT. All of the obtained results are found to be in match with the previously published results in [de Vahl Davis (1983); Colaço, Dulikravich and Orlande (2009)] and the results from FLUENT code. Advantages of the LRBFCM method are its accuracy, simplicity and straightforward implementation of the algorithm on non-uniform node arrangements as well as for involved physics.

In the future, the problems with externally applied magnetic field with inflow and outflow will be considered, as a next step towards the solution of the industrially relevant continuous casting of steel with externally applied magnetic field [Šarler, Vertnik and Mramor (2012)]. This paper represents the first step towards simulation of a spectra of industrial fluid flow problems which include electromagnetic fields by LRBFCM.

Acknowledgement

The research in this paper was sponsored by Centre of Excellence for Biosensors, Instrumentation and Process Control (COBIK) and the Slovenian Grant Agency under grant J2-4120 and programme P2-0379. COBIK is an operation financed by the European Union, European Regional Development Fund and Republic of Slovenia, Ministry of Education, Science, Culture and Sport. The present paper has been presented by the first author at 8th ICCES Special Symposium on Meshless & Other Novel Computational Methods, September 2-6, 2012, Maestral Hotel, Budva, Montenegro.

References

- An-Vo, D.A.; Mai-Duy, N.; Tran-Cong, T.** (2011a): A C2-continuous control-volume technique based on Cartesian grids and two-node integrated RBF elements for second-order elliptic problems. *CMES: Computer Modeling in Engineering and Sciences*, vol. 72, pp. 299-335.
- An-Vo, D.A.; Mai-Duy, N.; Tran-Cong, T.** (2011b): High-order upwind methods based on C2-continuous two-node integrated-RBF elements for viscous flows. *CMES: Computer Modeling in Engineering and Sciences*, vol. 80, pp. 141-177.

An-Vo, D.A.; Mai-Duy, N.; Tran, C.D.; Tran-Cong, T. (2013): ADI method based on C2-continuous two-node integrated-RBF elements for viscous flow. *Applied Mathematical Modeling*, vol. 37, pp. 5184-5203.

Atluri, S.N.; Shen, S. (2002): *The Meshless Method*. Tech Science Press, Encino.

Atluri, S.N. (2004): *The Meshless Method (MLPG) for Domain and Boundary Discretizations*. Tech Science Press, Encino.

Al-Najem, N.; Khanafer, K.; El-Refaee, M. (1998): Numerical study of laminar natural convection in tilted enclosure with transverse magnetic field. *International Journal of Numerical Methods for Heat and Fluid Flow*, vol. 8, pp. 651-672.

Arefmanesh, A.; Naja, M.; Nikfar, M. (2010): Meshless local Petrov-Galerkin simulation of buoyancy-driven fluid flow and heat transfer in a cavity with wavy side walls. *CMES: Computer Modeling in Engineering and Sciences*, vol. 62, pp. 113-149.

Bayona, V.; Moscoso, M.; Carretero, M.; Kindelan, M. (2010): RFB-FD formulas and convergence properties, *Journal of Computational Physics*, vol. 229, pp.8281-8295.

Bejan, A. (1995): *Convection Heat transfer*. John Wiley & Sons, Inc.

Buhmann, M. D. (2000): *Radial Basis Functions*. Cambridge University Press, Cambridge.

Cheng-Wen, Z.; Jian-Fei, X.; Cong-Shan, Z.; Sheng-Wei, X.; Da-Chuan, Y. (2009): Simulation of natural convection under high magnetic field by means of the thermal lattice Boltzmann method. *Chinese Physics B*, vol. 18, pp. 4083-4093.

Chorin, A. (1967): A numerical method for solving incompressible viscous flow problems. *Journal of Computational Physics*, vol. 2, pp. 12-26.

Colaço, M.; Dulikravich, G.; Orlande, H. (2009): Magnetohydrodynamic simulations using radial basis functions. *International Journal of Heat and Mass Transfer*, vol. 52, pp. 5932-5939.

Davidson, P. A.; Thess, A. (2002): *Magnetohydrodynamics*. vol. 418. Springer.

de Vahl Davis, G. (1983): Natural convection of air in a square cavity: a benchmark numerical solution. *International Journal for Numerical Methods in Fluids*, vol. 3, pp. 249-264.

Di Piazza, I.; Ciofalo, M. (2002): MHD free convection in a liquid-metal filled cubic enclosure. I. Differential heating. *International Journal of Heat and Mass Transfer*, vol. 45, pp. 1477-1492.

Di Piazza, I.; Ciofalo, M. (2002b): MHD free convection in a liquid-metal filled cubic enclosure. II. Internal heating. *International Journal of Heat and Mass*

Transfer, vol. 45, pp. 1493-1511.

Fasshauer, G.E. (2007): *Meshfree Approximation Methods with MATLAB, Interdisciplinary Mathematical Sciences*, vol. 6, World Scientific Publishers, Singapore.

Ferreira, A.; Roque, C.; Martins, P. (2003): Analysis of composite plates using higher-order shear deformation theory and a finite point formulation based on the multiquadric radial basis function method. *Composites Part B: Engineering*, vol. 34, pp. 627–636.

Fluent, I. (2003): FLUENT 6.1. User's Guide. Lebanon (NH), Fluent Inc.

Franke, R. (1982): Scattered data interpolation: Tests of some methods. *Mathematics of Computation*, vol. 38, pp. 181-200.

Garandet, J. P.; Alboussiere, T.; Moreau, R. (1992). Buoyancy driven convection in a rectangular enclosure with a transverse magnetic field. *International Journal of Heat and Mass Transfer*, vol. 4, pp. 741-748.

Gu, G.R.; Liu, Y. T. (2005): An Introduction to Meshfree Methods and Their Programming. *Springer, Dordrecht*.

Hon, Y.C.; Schaback R. (2001): On unsymmetric collocation by radial basis functions. *Applied Mathematics and Computation*, vol. 119, pp. 177-186.

Hanoglu, U.; Šarler, B. (2011): Thermo-Mechanical Analysis of Hot Shape Rolling of Steel by a Meshless Method. *Procedia Engineering*, vol. 10, 3173-3178.

Kansa, E. (1990a): Multiquadrics: A scattered data approximation scheme with applications to computational fluid-dynamics I surface approximations and partial derivative estimates. *Computers and Mathematics with Applications*, vol. 19, pp. 127-145.

Kansa, E. (1990b): Multiquadrics: A scattered data approximation scheme with applications to computational fluid-dynamics II solutions to parabolic, hyperbolic and elliptic partial differential equations. *Computers and Mathematics with Applications*, vol. 19, pp. 147-161.

Kaviany, M. (2001): *Principles of Convective Heat Transfer*. Springer.

Kosec, G.; Šarler, B. (2008a): Local RBF collocation method for Darcy flow. *CMES: Computer Modeling in Engineering and Sciences*, vol. 25, pp. 197-208.

Kosec, G.; Šarler, B. (2008b): Solution of thermo-fluid problems by collocation with local pressure correction. *International Journal of Numerical Methods for Heat and Fluid Flow*, vol. 18, pp. 868-882.

Kosec, G.; Šarler, B. (2009): Solution of phase change problems by collocation with local pressure correction. *CMES: Computer Modeling in Engineering and Sciences*, vol. 47, pp. 191-216.

Kosec, G.; Šarler, B. (2011): H-adaptive local radial basis function collocation meshless method. *CMC: Computers Materials and Continua*, vol. 26, pp. 227-253.

Kosec, G.; Založnik, M.; Šarler, B.; Combeau, H. (2011): A meshless approach towards solution of macrosegregation phenomena. *CMC: Computers Materials and Continua*, vol. 22, pp. 169-195.

Kosec, G.; Šarler, B. (2012): Solution of a low Prandtl number natural convection benchmark by a local meshless method. *International Journal of Numerical Methods for Heat & Fluid Flow*, vol. 23, pp. 189-204.

Kosec, G.; Zinterhof, P. (2013): Local strong form meshless method on multiple Graphics Processing Units. *CMES: Computer Modeling in Engineering and Sciences*, vol. 91, pp. 377-396.

Kovačević, I.; Šarler, B. (2005): Solution of a phase-field model for dissolution of primary particles in binary aluminum alloys by an r-adaptive mesh-free method. *Materials Science and Engineering*, vol. 413A, pp. 423-428.

Liu, G.R. (2010): *Meshfree methods. 2nd edition*. CRC Press, Boca Raton, FL.

Mai-Duy, N.; Tran-Cong, T. (2010): A control volume technique based on integrated RBFNs for the convection–diffusion equation. *Numerical Methods for Partial Differential Equations*, vol. 26, pp. 426-447.

Ngo-Cong, D.; Mai-Duy, N.; Karunasena, W.; Tran-Cong, T. (2012): Local moving least square-one-dimensional IRBFN technique: Part I - natural convection flows in concentric and eccentric annuli. *CMES: Computer Modeling in Engineering and Sciences*, vol. 83, no. 3, pp. 275-310.

Ngo-Cong, D.; Mai-Duy, N.; Karunasena, W.; Tran-Cong, T. (2012): Local moving least square-one-dimensional IRBFN technique: Part II - Unsteady incompressible viscous flows. *CMES: Computer Modeling in Engineering & Sciences*, vol. 83, no. 3, pp. 311-351.

Rudraiah, N.; Barron, R.; Venkatachalappa, M.; Subbaraya, C. (1995): Effect of a magnetic field on free convection in a rectangular enclosure. *International Journal of Engineering Science*, vol. 33, pp. 1075-1084.

Sadat, H.; Couturier, S. (2000): Performance and accuracy of a meshless method for laminar natural convection. *Numerical Heat Transfer*, vol. 4B, pp. 455-467.

Salah, N. B.; Soulaïmani, A.; Habashi, W. G. (2001): A finite element method for magnetohydrodynamics. *Computer Methods in Applied Mechanics and Engineering*, vol. 190, pp. 5867-5892.

Sarris, I.; Kakarantzas, S.; Grecos, A.; Vlachos, N. (2005): MHD natural convection in a laterally and volumetrically heated square cavity. *International Journal*

of Heat and Mass Transfer, vol. 48, pp. 3443-3453.

Sathiyamoorthy, M.; Chamkha, A. (2010): Effect of magnetic field on natural convection flow in a liquid gallium filled square cavity for linearly heated side wall(s). *International Journal of Thermal Sciences*, vol. 49, pp. 1856-1865.

Skala, J.; Barta, M. (2012): LSFEM implementation of MHD numerical solver. *Applied Mathematics*, vol. 3, pp. 1842-1850.

Šarler, B. (2005): A radial basis function collocation approach in computational fluid dynamics. *CMES: Computer Modeling in Engineering and Sciences*, vol. 7, pp. 185-193.

Šarler, B.; Vertnik, R. (2006): Meshfree explicit local radial basis function collocation method for diffusion problems. *Computers and Mathematics with Applications*, vol. 51, pp. 1269-1282.

Šarler, B.; Atluri, S.N. (2010): *Recent Studies in Meshless and Other Novel Computational Methods*. Tech Science Press, Encino.

Šarler, B.; Vertnik, R.; Mramor, K. (2012): A numerical benchmark test for continuous casting of steel. *IOP Conference Series: Materials Science and Engineering*, vol. 33., IOP Publishing. doi: 10.1088/1757-899X/33/1/012012.

Thai-Quang, N.; Mai-Duy, N.; Tran, C. D.; Tran-Cong, T. (2012): High-order alternating direction implicit method based on compact integrated-RBF approximations for unsteady/steady convection-diffusion equations. *CMES: Computer Modeling in Engineering & Sciences*, vol. 89, no. 3, pp. 189-220.

Thai-Quang, N.; Le-Cao, K.; Mai-Duy, N.; Tran-Cong, T. (2012): A high-order compact local integrated-RBF scheme for steady-state incompressible viscous flows in the primitive variables. *CMES: Computer Modeling in Engineering and Sciences*, vol. 84, no. 6, pp. 528-557.

Vertnik, R.; Šarler, B. (2006): Meshless local radial basis function collocation method for convective-diffusive solid-liquid phase change problems. *International Journal of Numerical Methods for Heat and Fluid Flow*, vol. 16, pp. 617-640.

Vertnik, R.; Šarler, B. (2009): Solution of incompressible turbulent flow by a mesh-free method. *CMES: Computer Modeling in Engineering & Sciences*, vol. 44, pp. 65-96.

Vertnik, R.; Šarler, B. (2011): Local collocation approach for solving turbulent combined forced and natural convection problems. *Advances in Applied Mathematics and Mechanics*, vol. 3, pp. 259-279.

Vertnik, R.; Šarler, B.; Senčič, B. (2011): Solution of macrosegregation in continuously cast billets by a meshless method. *IOP Conference Series: Materials Science and Engineering*, vol. 27, pp. 2058. IOP Publishing.

Vertnik, R.; Založnik, M.; Šarler, B. (2006): Solution of transient direct-chill aluminium billet casting problem with simultaneous material and interphase moving boundaries by a meshless method. *Engineering Analysis with Boundary Elements*, vol. 30, pp. 847–855.

Wendland, H. (2005): *Scattered Data Approximation*. Cambridge University Press, Cambridge.

Wright, G.B; Fornberg, B. (2006): Scattered node compact finite difference-type formulas generated from radial basis function. *Journal of Computational Physics*, vol. 212, pp. 1623-1648.